

1 *Supplement materials to the manuscript titled* **“Mixing state, spatial**  
2 **distribution, sources and photochemical enhancement to**  
3 **sulfate formation of black carbon particles in the Arctic**  
4 **Ocean during summer”**

5

6 Longquan Wang<sup>1,2</sup>, Jinpei Yan<sup>3</sup>, Afeng Chen<sup>1,4</sup>, Bei Jiang<sup>1,5</sup>, Fange Yue<sup>1</sup>, Xiawei Yu<sup>1</sup>,  
7 Zhouqing Xie<sup>1,6\*</sup>

8

9 <sup>1</sup>Anhui Key Laboratory of Polar Environment and Global Change, Department of Environmental Science  
10 and Engineering, University of Science and Technology of China, Hefei 230026, China.

11 <sup>2</sup>Department of Carbon Neutral Science and Engineering, Anhui University of Science and Technology,  
12 Hefei 230026, China.

13 <sup>3</sup>Third Institute of Oceanography, Ministry of Natural Resources, Xiamen 361005, China.

14 <sup>4</sup>Engineering and Technological Research Centre of National Disaster Relief Equipment, Army Logistics  
15 Academy, Chongqing, 401331, China.

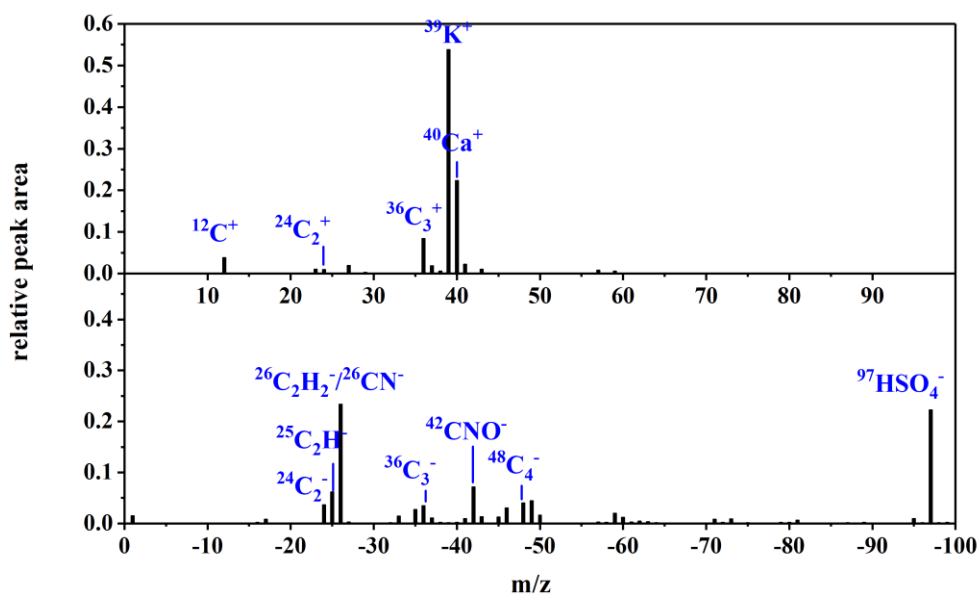
16 <sup>5</sup>College of Ecology and Environment, Xinjiang University, Urumqi, 830017, PR China.

17 <sup>6</sup>State Key Laboratory of Fire Science, University of Science and Technology of China, Hefei, 230026,  
18 China.

19 *Correspondence to:* Zhouqing Xie (zqxie@ustc.edu.cn)

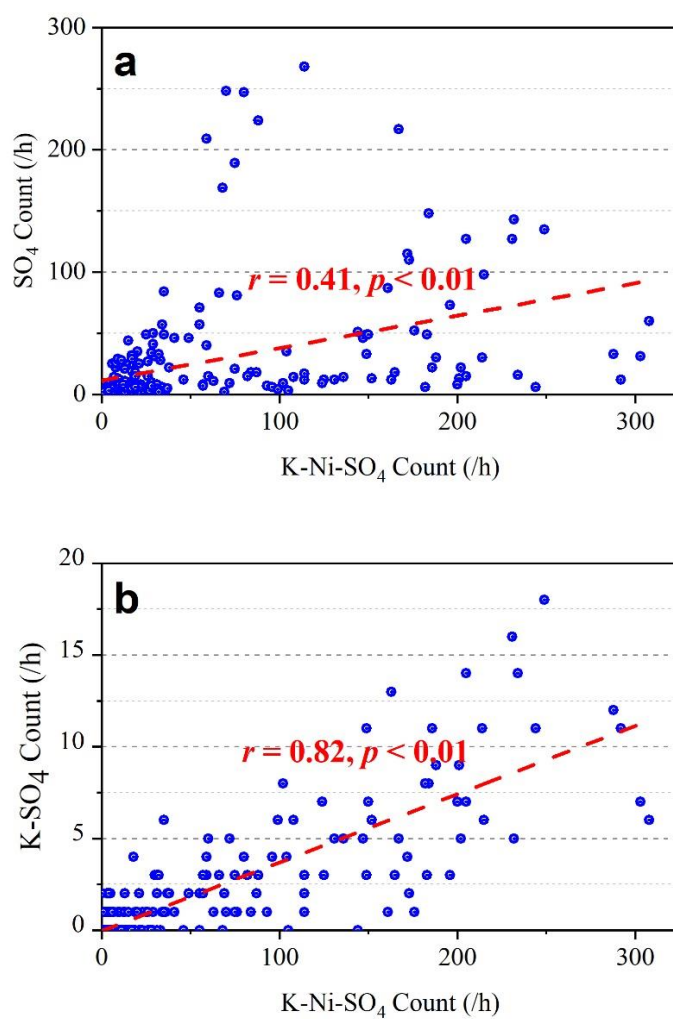
20

21



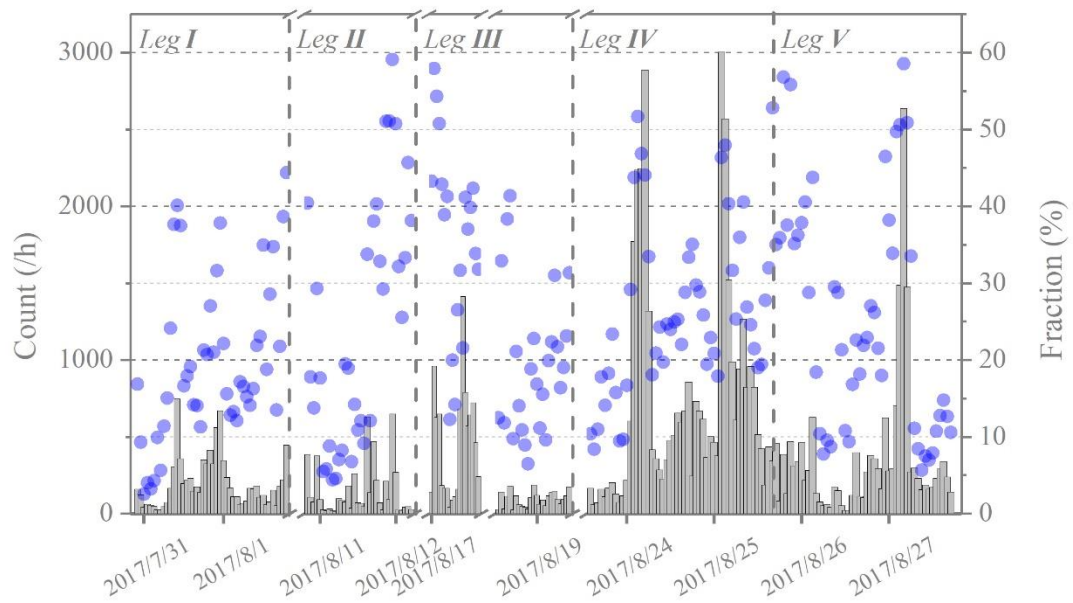
22

23 **Figure S1.** Average map of black carbon particles, with peaks showing strong signals marked in  
 24 blue. The X-axis represents the mass-to-charge ratio ( $m/z$ ), and the Y-axis indicates the relative peak  
 25 area. The upper half of the map displays the cation spectrum, while the lower half shows the anion  
 26 spectrum. In the cation spectrum, peaks for  $^{39}\text{K}^+$  and  $^{40}\text{Ca}^+$  are identified, excluding inorganic carbon  
 27 peaks ( $^{12}\text{C}^+$ ,  $^{24}\text{C}_2^+$  and  $^{36}\text{C}_3^+$ ). In the anion spectrum, peaks for inorganic carbon ( $^{24}\text{C}_2^-$ ,  $^{36}\text{C}_3^-$  and  
 28  $^{48}\text{C}_4^-$ ), organic carbon ( $^{25}\text{C}_2\text{H}^-/^{26}\text{C}_2\text{H}_2^-$ ,  $^{26}\text{CN}^-/^{42}\text{CNO}^-$ ), and  $^{97}\text{HSO}_4^-$  are identified.



29

30 **Figure S2.** Relationship between K-Ni-SO<sub>4</sub> and SO<sub>4</sub>, as well as K-SO<sub>4</sub> black carbon particles. The  
31 X-axis represents the hourly count of K-Ni-SO<sub>4</sub> black carbon particles. The Y-axis shows the hourly  
32 count of SO<sub>4</sub> black carbon particles in the upper graph and K-SO<sub>4</sub> black carbon particles in the lower  
33 graph, respectively. A red dashed line indicates the linear fit curve, with the correlation coefficient  
34 ( $r$ ) and significance level ( $p$ ) provided.



35

36 **Figure S3.** Hourly counts and fractions of black carbon particles from Leg I to Leg V. The X-axis

37 displays the sampling time. Gray columns represent the hourly counts of black carbon particles,

38 while blue dots indicate the hourly fractions of black carbon particles relative to all particles. Each

39 segment of the cruise is delineated by a dotted line.

40 **Table S1.** Sampling time (in UTC) and locations during the cruise (Jul: July; Aug: August; lon:  
41 longitude; lat: latitude)

|                | Sampling Time  |                | Starting Location |        | Ending Location |        |
|----------------|----------------|----------------|-------------------|--------|-----------------|--------|
|                | start          | end            | lon               | lat    | lon             | lat    |
| <b>Leg I</b>   | 22:00 30th Jul | 19:00 1st Aug  | 169.4°W           | 66.0°N | 159.2°W         | 74.8°N |
| <b>Leg II</b>  | 20:00 10th Aug | 5:00 12th Aug  | 132.0°E           | 83.7°N | 110.4°E         | 84.6°N |
| <b>Leg III</b> | 2:00 17th Aug  | 11:00 19th Aug | 25.4°E            | 82.6°N | 2.1°E           | 74.3°N |
| <b>Leg IV</b>  | 14:00 23th Aug | 14:00 25th Aug | 2.1°W             | 67.0°N | 25.8°W          | 61.2°N |
| <b>Leg V</b>   | 14:00 25th Aug | 17:00 27th Aug | 25.9°W            | 61.1°N | 46.9°W          | 56.2°N |

42